Improved Tropical Storm Forecasts with *GOES-13/15* Imager Radiance Assimilation and Asymmetric Vortex Initialization in HWRF

X. ZOU

Earth System Science Interdisciplinary Center, University of Maryland, College Park, College Park, Maryland

Z. QIN

Nanjing University of Information Science and Technology, Nanjing, China, and Earth System Science Interdisciplinary Center, University of Maryland, College Park, College Park, Maryland

Y. ZHENG

Chinese Academy of Meteorological Sciences, China Meteorological Administration, Beijing, China, and Earth System Science Interdisciplinary Center, University of Maryland, College Park, College Park, Maryland

(Manuscript received 3 July 2014, in final form 23 February 2015)

ABSTRACT

The Geostationary Operational Environmental Satellite (GOES) imagers provide high temporal- and spatial-resolution data for many applications, such as monitoring severe weather events. In this study, radiance observations of four infrared channels from *GOES-13* and *GOES-15* imagers are directly assimilated using the National Centers for Environmental Prediction (NCEP) gridpoint statistical interpolation (GSI) analysis system to produce the initial conditions for the Hurricane Weather Research and Forecasting Model (HWRF). Impacts of GOES imager data assimilation on track and intensity forecasts are demonstrated for a landfalling tropical storm that moved across the Gulf of Mexico—Debby (2012). With a higher model top and a warm start, an asymmetric component is also added to the original HWRF symmetric vortex initialization. Two pairs of data assimilation and forecasting experiments are carried out for assessing the impacts of the GOES imager data assimilation on tropical storm forecasts. The first pair employs a symmetric vortex initialization and the second pair includes an asymmetric vortex initialization. Numerical forecast results from these experiments are compared against each other. It is shown that a direct assimilation of *GOES-13* and *GOES-15* imager radiance observations, which are available at all analysis times, in HWRF results in a consistently positive impact on the track and intensity forecasts of Tropical Storm Debby in the Gulf of Mexico. The largest positive impact on the track and intensity forecasts comes from a combined effect of GOES imager radiance assimilation and an asymmetric vortex initialization.

1. Introduction

Tropical cyclones spend most of their times over oceans, where they are rarely observed by conventional data. Currently, observations of tropical cyclones over oceans rely primarily on airborne and satellite data. The Geostationary Operational Environmental Satellite (GOES) imager instruments provide nearly continuous, high-horizontal-resolution observations at one visible and four infrared channels over storm domains. Thus, the GOES data are unique for capturing fast-evolving weather systems at all relevant scales (Stengel et al. 2009; Zou et al. 2011). It is important to fully utilize GOES data to improved hurricane forecasts. In this study, the four infrared channels' radiance data from *GOES-13* and *GOES-15* satellites are assimilated into the Hurricane Weather Research and Forecasting Model (HWRF) for the first time and the impacts on tropical storm-track and intensity forecasts are evaluated.

Satellite data assimilation has been an active area of research for operational global numerical weather prediction (NWP) systems since the 1990s. Passive infrared

Corresponding author address: Dr. Xiaolei Zou, Earth System Science Interdisciplinary Center, University of Maryland, College Park, 5825 University of Maryland Research Court, Office 4078, College Park, MD 20740-3823.
E-mail: xzou1@umd.edu

DOI: 10.1175/MWR-D-14-00223.1

© 2015 American Meteorological Society

and microwave channel radiance observations from various polar-orbiting satellite instruments have been routinely assimilated into NWP systems at almost all operational centers including the National Centers for Environmental Prediction (NCEP) and the European Centre for Medium-Range Weather Forecasts (ECMWF) since the late 1980s (Eyre et al. 1993; Andersson et al. 1994; Derber and Wu 1998; McNally et al. 2006). Significant improvements in global NWP forecasts have been obtained from a direct assimilation of radiance observations instead of their retrieved temperature and water vapor profiles (Eyre et al. 1993; Andersson et al. 1994; Derber and Wu 1998). Migliorini (2012) pointed out that direct assimilation of satellite radiance measurements is equivalent to assimilating the satellite retrieval products if the following requirements were met: (i) the forward radiative transfer model is approximately linear near a state space centered at the retrieval temperature within an interval on the order of the retrieval error; and (ii) any prior information used for constraining the satellite retrieval should not underrepresent the variability of the atmospheric state in order to properly retain the information content of the measurements.

Advances in satellite data assimilation for tropical cyclone prediction had been relatively slow. Early studies on satellite data assimilation for improved vortex initialization and hurricane prediction included those using a four-dimensional variational data assimilation (4D-Var) approach with either the fifth-generation Pennsylvania State University–National Center for Atmospheric Research Mesoscale Model (MM5) (Zou and Xiao 2000; Zou et al. 2001; Zhu et al. 2002) or the Coupled Ocean–Atmosphere Mesoscale Prediction System (COAMPS) atmospheric model (Amerault and Doyle 2008; Amerault et al. 2009). Besides satellite instruments, hurricanes were frequently observed by airborne radars in the United States. Through a case study, Pu et al. (2009) showed that assimilation of airborne radar reflectivity and radial wind data had greatly improved the thermal and hydrometeor structures of an initial vortex, leading to improved precipitation structures, and track and intensity changes of Hurricane Dennis (2005) in the subsequent forecasts. Recently, Zhang and Weng (2015) showed that the day 2–to–day 4 intensity forecast errors could be reduced by 25%–28% compared to the corresponding National Hurricane Center's official forecasts. In the study of Zhang and Weng (2015), ensemble data assimilation techniques were employed for ingesting high-resolution inner-core airborne Doppler radar observations for over all 102 applicable cases during 2008–12.

Assimilation of radiance observations from various remote sensing instruments on board polar-orbiting satellites had significantly improved the forecast skills of global NWP models (Eyre et al. 1993; Andersson et al. 1994). Assimilation of GOES radiance observations lagged behind the assimilation of radiances from polar-orbiting satellites for several reasons. Although they have high temporal and spatial resolutions, geostationary instruments provide low-spectral-resolution (e.g., a few channels) infrared radiance measurements, single visible channel observations, and limited observing domains. Early use of GOES observations focused on atmospheric motion winds that were derived by tracking the cloud or water vapor features from infrared channels in sequential satellite images[1] (Nieman et al. 1993; Velden 1996; Velden et al. 1997). Assimilation of GOES-derived water vapor or cloud-tracked winds was carried out that had demonstrated some positive or neutral impacts on NWP (Goerss et al. 1998; Velden et al. 1998; Tomassini et al. 1999; Soden et al. 2001). Only more recently than the routine exercise of assimilating radiances from polar-orbiting satellites into operational global forecast systems, GOES radiances were directly assimilated to avoid a major shortcoming with the assimilation of GOES winds—a well-known uncertainty in the height assignment of GOES-derived winds (Rao et al. 2002). Efforts to incorporate radiance observations from geostationary satellites into global and regional NWP systems included studies by Köpken et al. (2004) for the Meteosat Visible and Infrared Imager (MVIRI) on board *Meteosat-7*, Szyndel et al. (2005) and Stengel et al. (2009) for the Spinning Enhanced Visible and Infrared Imager (SEVIRI) on board *Meteosat-8*, Su et al. (2003) for the GOES imager of the United States for global data assimilation, and Zou et al. (2011) and Qin et al. (2013) for the GOES imager on board *GOES-11* and *GOES-12* of the United States for regional quantitative precipitation forecasts (QPFs). In Zou et al. (2011), the NCEP gridpoint statistical interpolation (GSI) analysis system was employed for GOES data assimilation experiments and the Advanced Research version of WRF (ARW) was used for short-range (e.g., 24–36 h) forecasts. Assimilation of GOES imager radiances during a 12-h or slightly longer time window prior to convective initiation and development could significantly improve QPFs near the coast of the northern Gulf of Mexico (Zou et al. 2011). Qin et al. (2013) proceeded to assess the benefits of adding *GOES-11/12* imager infrared channel radiances to the assimilation of other satellite data, including the Advance Microwave Sounding Unit A (AMSU-A), the

[1] http://www.star.nesdis.noaa.gov/smcd/opdb/goes/winds/wind.html.

TABLE 1. *GOES-13* and *GOES-15* imager channel center frequency, bandwidth, data resolution at the subsatellite point, and data noise at 300 K for channels 1, 2, 4, and 6 and data noise at 230 K for channel 3.

			Data resolution (km)		Data noise (K)	
Channel No.	Center frequency (μm)	Bandwidth (μm)	*GOES-13*	*GOES-15*	*GOES-13*	*GOES-15*
1	0.65	0.19	1.0	1.0	±5%	±5%
2	3.90	0.34	4.0	4.0	0.051	0.063
3	6.55	1.50	4.0	4.0	0.14	0.17
4	10.7	1.00	4.0	4.0	0.053	0.059
6	13.35	0.70	8.0	4.0	0.061	0.13

hyperspectral Atmospheric Infrared Sounder (AIRS), the High Resolution Infrared Radiation Sounder (HIRS), GOES Sounder (GSN), the Advance Microwave Sounding Unit B (AMSU-B), and the Microwave Humidity Sounder (MHS) data in GSI and ARW. It was shown that convection-induced QPFs near the Gulf Coast could be further improved by adding GOES data to other satellite data.

The present study incorporates *GOES-13* and *-15* infrared channel radiance data into the HWRF system with two different schemes for vortex initialization and assesses the impacts of *GOES-13* and *-15* data on tropical storm prediction. The modified 2012 version of the HWRF system is employed for this study. Major modifications include a higher model top and a warm start, which were described in Zou et al. (2013), who conducted a preliminary study on satellite data assimilation for tropical cyclone prediction using this modified HWRF system. They demonstrated a consistent, positive impact of assimilating radiance observations from a new microwave instrument, the Advanced Technology Microwave Sounder (ATMS) on board the *Suomi–National Polar-Orbiting Partnership* (*SNPP*) satellite, on forecasts of four Atlantic hurricane cases that made landfall in 2012.

This paper is organized as follows: Imager channel characteristic features of *GOES-13* and *-15* are briefly described in section 2. The HWRF vortex initialization and an addition of an asymmetric component are presented in section 3. The HWRF model, the NCEP GSI data analysis system, and the numerical experiment setup are provided in section 4. Asymmetric vortex structures and analysis increments from *GOES-13/15* imager radiance assimilation are presented and discussed in section 4. In section 5, impacts of GOES data assimilation on track and intensity forecasts are shown. A summary and conclusions are provided in section 6.

2. GOES data characteristics

GOES-13 and *-15* satellites are the two operational GOES systems operated by the U.S. National Oceanic and Atmospheric Administration (NOAA) National Environmental Satellite, Data, and Information Service (NESDIS). NOAA *GOES-14* remains in orbital storage. *GOES-13* became the official GOES-East satellite on 14 April 2010, replacing *GOES-12*. *GOES-15* replaced *GOES-11* on 6 December 2011 and became NOAA's GOES-West satellite. Specifically, the *GOES-13* and *-15* satellites are positioned in geostationary orbits at 75° and 135°W, respectively. Both satellites are perched 35 800 km above the equator to spot potentially life-threatening weather, including tropical storm activity in the Atlantic Ocean, the Gulf of Mexico, and the Pacific Ocean, at a full earth imaging refresh rate of 26 min.[2] The observations from GOES satellites are not only used for weather applications but also for tracking space weather, oceanographic changes, forest fires, and other hazards, and for search and rescue operations. Tropical Storm Debby (2012), which moved in a relatively data-void region in the Gulf of Mexico, was well sampled by *GOES-13* and *-15* and will be used for investigating the potential impacts of GOES data assimilation for tropical storm prediction in this study.

Both *GOES-13* and *-15* imagers have five channels. Table 1 provides center frequency; bandwidth; resolution at the subsatellite point; noise at 300 K for channels 1, 2, 4, and 6; and noise at 230 K for channel 3. Both *GOES-13* and *-15* imagers have one visible channel with a center wavelength of 0.65 μm (channel 1), and four infrared channels consisting of a shortwave infrared window channel with its wavelength centered at 3.9 μm (channel 2), an infrared water vapor channel located at 6.5 μm (channel 3), a longwave infrared window channel centered at 10.7 μm (channel 4), and a longwave infrared carbon dioxide channel whose wavelength is located at 13.3 μm (channel 6). The spatial resolution (i.e., instantaneous geometric field of view) of the visible channel is 1 km and that of the infrared channels is 4 km at the subsatellite point, except

[2] http://www.nasa.gov/mission_pages/goes-n/media/goes-east.html.

for *GOES-13* channel 6. The *GOES-13* imager channel 6 has a coarser resolution (8 km) than the spatial resolution (4 km) of channel 6 from *GOES-15*. Since the resolution of *GOES-15* channel 6 matches that of the other three infrared channels on board the same satellite, it is apparently beneficial for assimilating *GOES-15* multichannel radiance data and for deriving *GOES-15* multichannels products than its predecessors *GOES-12* and *-13*.

The five GOES channels are designed for different purposes. The visible channel 1 observes the reflected radiation from the earth and therefore is ideal for detecting clouds, aerosols, and surface features during daytime. Channel 2 provides unique cloud detection capabilities that greatly enhance the ability to analyze cloud patterns and a variety of terrestrial features, most notably fires, hot spots, and snow coverage. Channel 3 is mainly used for depicting both water vapor and clouds in the mid- and upper levels of the atmosphere, since the earth's emitted spectrum at channel 3's wavelength of 6.5 μm is highly attenuated by water molecules. The 4-km spatial resolution of channel 3 at the satellite subpoint for both *GOES-13* and *-15*, compared with 8 km for their predecessors *GOES-11* and *-12*, can also aid in the depiction of smaller-scale features such as jet streaks and cloud streaks, as well as banded clouds and precipitation. At the wavelength of channel 4 (10.7 μm), most surfaces and cloud types have an emissivity close to 1 and the energies emitted by the earth's surface or cloud are not significantly attenuated by the atmospheric gases. Therefore, brightness temperatures at channel 4 measured by the GOES satellite are close to actual surface skin or cloud-top temperatures except for thin cirrus. In contrast to channel 4, channel 6 is located within a region of the earth's emitted spectrum (13.3 μm) where a considerable amount of both cloud- and surface-emitted radiation is attenuated by carbon dioxide molecules.

3. Vortex initialization

a. Symmetric vortex initialization

The vortex initialization in the HWRF 2012 version is performed at the 9-km-resolution domain. The model fields in the 3-km-resolution domain are downscaled from those over the 9-km domain. The symmetric vortex initialization that was implemented in the HWRF system consists of the following five major steps: (i) determining the storm center based on tropical cyclone vital statistics (TCVitals) records; (ii) decomposing Global Forecast System (GFS) 6-h forecast fields into the following three components: a basic field, a nonhurricane disturbance field, and a hurricane disturbance field (Kurihara et al. 1993, 1995); (iii) replacing the hurricane disturbance field extracted from the GFS field in the previous step [(ii)] by one of the two prespecified symmetric bogus vortices: one for deep vortex and one for shallow or medium; (iv) applying a storm size correction and an intensity correction to the prespecified vortex fields according to the available storm size and intensity data provided by the Tropical Prediction Center (TPC) for the tropical cyclone to be initialized in the HWRF model; and (v) adjusting surface pressure, temperature, and water vapor mixing ratio fields accordingly. A detailed description of the HWRF vortex initialization can be found in Bao et al. (2012) and Gopalakrishnm et al. (2012).

The sum of the basic field and nonhurricane disturbance field is called the environmental field. The sum of the environmental field and the corrected initial bogus vortex is then used as the background field for conventional and satellite data assimilation. The data assimilation is repeated at a 6-h interval. To eliminate complications associated with double uses of data, the 6-h HWRF forecasts are used as the background fields instead of the GFS 6-h forecast field for extracting the environmental fields after the first cycle of data assimilation.

b. Asymmetric vortex initialization

Most tropical cyclones exhibit asymmetric structures. An asymmetric structure plays a significant role in the tropical cyclone motion. If no asymmetry is present in the initial condition, then a long time (1–2 days) is required before the vortex exhibits quasi-steady propagation due to the beta effect (Kurihara et al. 1993; Bender et al. 1993). Since the planetary vorticity advection by the symmetric flow within the vortex is one of many factors that influence the development of asymmetric structure in TCs, Kurihara et al. (1993) and Bender et al. (1993) proposed to obtain an asymmetric component of wind from integrating a barotropic vorticity equation from the symmetric vortex as its initial condition. Their method is employed in this study.

The barotropic vorticity model consists of integrating the following equation:

$$\frac{\partial(\varsigma + f)}{\partial t} + \mathbf{v} \cdot \nabla(\varsigma + f) = 0, \tag{1}$$

$$\mathbf{v} = \mathbf{k} \times \nabla\psi, \tag{2}$$

and

$$\nabla^2\psi = \varsigma, \tag{3}$$

where ς is relative vorticity, ψ is streamfunction, $\mathbf{v}$ is velocity, $f = 2\Omega \sin\varphi$ is the Coriolis parameter, $\Omega = 7.292 \times 10^{-5}\,\mathrm{s}^{-1}$ is the earth's rotation rate, and φ represents the latitude.

Eqs. (1)–(3) are solved numerically in a two-dimensional (2D) horizontal β plane through a spectral expansion. The β plane is defined by a square area $[-L_x, L_x]$ and $[-L_y, L_y]$ of 256×256 grids with a grid spacing of 10 km. The center of the square area is placed at the center of a vortex. The streamfunction variable (ψ) can be approximated by a truncated 2D Fourier series as follows:

$$\psi(x,y) = \sum_{n=-N/2}^{N/2} \sum_{m=-M/2}^{M/2} \psi_{mn} e^{i\pi[(mx/L_x)+(ny/L_y)]} \quad (4)$$

where the spectral coefficients ψ_{mn} of the mth wavenumber in the x direction and the nth wavenumber in the y direction is defined by

$$\psi_{mn} = \sum_{j=1}^{N} \sum_{i=1}^{M} \psi(x_i, y_j) e^{-i\pi[(mx_i/L_x)+(ny_j/L_y)]} \quad (5)$$

Substituting Eq. (4) into Eqs. (1)–(3), one obtains the following equations for the spectral coefficients of streamfunction (ψ_{mn}), relative vorticity (ς_{mn}), zonal wind (u_{mn}) and meridional wind (v_{mn}):

$$\frac{\partial \zeta_{mn}}{\partial t} + [\nabla \cdot \mathbf{v}(\zeta + f)]_{mn} = 0 \quad (6)$$

$$u_{mn} = -\frac{i\pi n}{L_y}\psi_{mn}, \quad v_{mn} = +\frac{i\pi m}{L_x}\psi_{mn}, \quad (7)$$

and

$$\psi_{mn}\left(-\frac{m^2\pi^2}{L_x^2} - \frac{n^2\pi^2}{L_y^2}\right) = \zeta_{mn}. \quad (8)$$

The Runge–Kutta time-marching method is used for the integration of Eq. (6) using a time step of $\Delta t = 120$ s, that is,

$$\begin{cases} \zeta_{mn}^1 = \zeta_{mn}^t - \Delta t A_{mn}^t \\ \zeta_{mn}^2 = \frac{3}{4}\zeta_{mn}^t + \frac{1}{4}(\zeta_{mn}^1 - \Delta t A_{mn}^1) \\ \zeta_{mn}^{t+1} = \frac{1}{3}\zeta_{mn}^t + \frac{2}{3}(\zeta_{mn}^2 - \Delta t A_{mn}^2), \end{cases} \quad (9)$$

where $A_{mn} = (i\pi m/L_x)(\varsigma_{mn} + f)u_{mn} + (i\pi n/L_y)(\varsigma_{mn} + f)v_{mn}$ for brevity.

The barotropic model [Eq. (9)] is integrated for 48 h with the HWRF symmetric vortex as its initial condition. The wind field obtained at the end of the barotropic vorticity model integration is taken as the asymmetric component of the bogus vortex and is added to the environmental field to produce the wind field of the asymmetric vortex. The vortex mass fields (pressure, geopotential, and temperature fields) are adjusted based on the divergence equation already incorporated into the HWRF initialization scheme (Kurihara et al. 1993; Bender et al. 1993). In summary, the asymmetric structure of the initial vortex that is added to the HWRF vortex initialization is determined from the symmetric vortex structure by a barotropic model.

4. Data assimilation and forecast systems

a. The HWRF system

The triply nested 2012 version of the HWRF system is used for this study. It has a nonhydrostatic mesoscale model dynamic solver (Janjić et al. 2001; Janjić 2003) and a triply nested domain configured with a parent domain of 27-km horizontal resolution with about 750×750 model grid points, an intermediate two-way telescopic moving nesting domain at 9 km with about 238×150 grid points, and an innermost two-way telescopic moving nesting domain at 3 km with about 50×50 grid points (Zhang et al. 2011). Both the intermediate and innermost domains are centered at an initial storm location and configured to follow the projected path of the storm. The original 2012 version HWRF had 43 hybrid vertical levels with more than 10 model levels being located below 850 hPa and a model top placed at about 50 hPa. To include many upper-level ATMS channels with their weighting functions peaking in the upper troposphere and stratosphere, the model top is raised to 0.5 hPa, and model levels are increased from 43 to 61 accordingly (Zou et al. 2013).

The HWRF atmospheric model employs the Ferrier microphysics, the NCEP GFS boundary layer physics, the GFS simplified Arakawa–Shubert deep convection, and the GFS shallow convection (Gopalakrishnan et al. 2012). The HWRF system also includes the Geophysical Fluid Dynamics Laboratory (GFDL) land surface model and radiation physics to account for air–sea interactions over warm water and/or under high wind conditions. The atmosphere component is also coupled to the Princeton Ocean Model (POM), which employs a feature-based initialization of loop current, warm and cold core eddies, and cold wake during the spinup phase of tropical cyclones.

b. The data assimilation system

The GSI analysis system is a three-dimensional variational data assimilation (3D-Var) system. An overview of the theory and the technical details of the GSI can be found in Wu et al. (2002). By constructing appropriate recursive filters into the analysis system, the spectral representation of the background error covariance in the spectral statistical interpolation (SSI) analysis system is replaced with a gridpoint representation to allow situation-dependent, anisotropic, and nonhomogeneous structures be built into the background error covariance matrix. The GSI thus adapts more flexibly to large inhomogeneous density and quality of different types of observations than its predecessor—the SSI analysis system at NCEP (Derber and Wu 1998). Details of the recursive filter techniques can be found in Wu et al. (2002) and Purser et al. (2003a,b). The GSI User's Guide[3] provides a step-by-step procedure to install, compile, and run the GSI on different local computer systems. The GSI had been successfully ported to a Linux platform at Florida State University (FSU), and the results in this study were obtained from the FSU local computing facilities.

The Community Radiative Transfer Model (CRTM) was employed as the observation operators for satellite data assimilation in the GSI. It was developed by the U.S. Joint Center for Satellite Data Assimilation (JCSDA) for rapid forward simulations of satellite radiances under various atmospheric and surface conditions. The CRTM and its adjoint operator were incorporated into the GSI. The CRTM supports a large number of sensors, including the historical, current (*GOES-13*, *-15*, etc.), and near-future sensors from the Geostationary Operational Environmental Satellite-R Series (GOES-R) and the Joint Polar Satellite System (JPSS), and covers the microwave, infrared, and visible frequency regions. More details on CRTM can be found in Weng (2007) and Han et al. (2007).

In the GSI, the observation weights for channels 2, 3, 4, and 6 of *GOES-13/15*, w_i (i = 2, 3, 4, and 5), are first given the following initial values of 2.0, 1.4, 3.0, and 3.0, respectively, which are the inverse of the square of the observation error variances. These values for the observation weights are then modified based on surface emissivity and surface temperature. Specifically, the initial value of the observation weight for channel 3, w_3, is reduced based on the standard deviation (δ_3) of GOES radiance data, which have a 4-km resolution, within a 40 km × 40 km grid box as follows:

$$w_3' = \begin{cases} w_3/1.0, & \delta_3 \le 0.4 \\ w_3/1.05, & 0.4 < \delta_3 \le 0.5 \\ w_3/1.09, & 0.5 < \delta_3 \le 0.6 \\ w_3/1.14, & 0.6 < \delta_3 \le 0.7 \\ w_3/1.17, & 0.7 < \delta_3 \le 0.8 \\ w_3/1.19, & 0.8 < \delta_3 \le 1.1 \\ w_3/1.25, & 1.1 < \delta_3 \le 1.3 \\ w_3/1.29, & 1.3 < \delta_3 \end{cases}.$$

It is reminded that GOES radiance data at 4-km resolution were thinned to a 40-km resolution for data assimilation. For other channels, $w_i' = w_i$ ($i \neq 3$).

Then, the observation weights are further modified based on different surface conditions in relation to surface emissivity and surface temperature:

$$w_i^f = \frac{w_i'}{1 + w_i' \times (f_\varepsilon \times |\varepsilon_i| + f_T \times |T_s|)^2},$$

where ε_i is the surface emissivity of the ith channel, T_s represents the surface air temperature, and the parameter f_ε is set to the following values according to surface type:

$$f_\varepsilon = \begin{cases} 0.01, & \text{sea and land} \\ 0.02, & \text{other surfaces} \end{cases},$$

$$f_\varepsilon = \begin{cases} 0.5, & \text{sea} \\ 2.0, & \text{land} \\ 3.0, & \text{ice and snow} \\ 5.0, & \text{other surfaces} \end{cases}.$$

GOES-13/15 radiance data assimilated in the GSI system include channels 2, 4, and 6 over sea, and channel 3 over both sea and land. Observations over ice, snow, and other surfaces are not assimilated in the current GSI.

The weights of channels 2, 4, and 6 over sea are nearly constant, which are 0.23, 0.11, and 0.11, respectively. The weight for channel 3 is shown in Fig. 1. The observation weights for channel 3 data over sea are mostly around 0.53. Observations weights for channel 3 over land vary more with the surface type and the temperature than those over sea.

c. Experiment setup

Two pairs of data assimilation and forecast experiments were carried out to assess the impacts of GOES data assimilation on tropical storm forecasts. As mentioned before, the vortex initialization is performed at the 9-km resolution domain. At 1800 UTC 23 June 2012, which is the starting time for initializing Tropical Storm

[3] http://www.dtcenter.org/com-GSI/users/index.php.

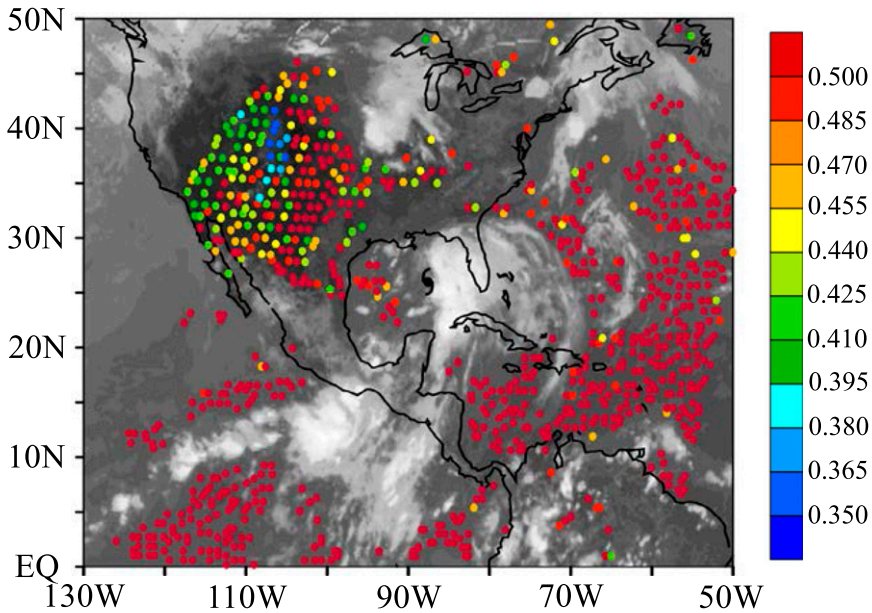

FIG. 1. Spatial distributions of observation weights for *GOES-13* channel 3 observations at 1800 UTC 23 Jun 2012.

Debby, a bogus vortex is merged with an environmental field extracted from the GFS analysis. The merged field is used as the background field for data assimilation of both conventional and satellite observations at the 9-km resolution domain. After the starting time, the 6-h HWRF forecasts are used for the environmental fields for the vortex initialization and data assimilation repeated at 6-h intervals to avoid complications associated with double uses of data. The vortex initialization and data assimilation are carried out from 1800 UTC 23 June to 1200 UTC 25 June. The model fields in the 3-km resolution domain are downscaled from those over the 9-km domain. During the time period from 1800 UTC 23 June to 1200 UTC 25 June, 5-day model forecasts are made in the triply nested HWRF domain described in section 4a at 6-h intervals as soon as the data assimilation is completed.

In the first pair of numerical experiments (CONTROL-S and GOES-S), the HWRF symmetric vortex initialization is used (Table 2). In the second pair of numerical experiments (CONTROL-AS and GOES-AS), a new asymmetric vortex initialization is used (Table 2). In all four experiments, conventional data, global positioning system (GPS) radio occultation (RO) data, Advanced Scatterometer (ASCAT) surface wind data, AMSU-A, AIRS, and HIRS data are assimilated into the HWRF parent and intermediate domains. The decision of including only radiance observations from AMSU-A, AIRS, and HIRS instruments but not MHS and GSN data was made based on a series of data-denying experiments conducted by Qin et al. (2013). Qin et al. (2013) showed that inclusions of MHS and GSN data in an all-satellite-data assimilation experiment degraded the forecast skill. The GOES-S experiment is the same as CONTROL-S except for adding *GOES-13* and *-15* imager data into the assimilation. The GOES-AS experiment is the same as GOES-S except for using an asymmetric vortex initialization.

5. Numerical results

a. *Asymmetric vortex structure*

Figure 2 shows the streamfunction and wind vector near the surface (e.g., 950 hPa) of the symmetric (Fig. 2a) and asymmetric (Fig. 2b) vortices at 1800 UTC 23 June 2012, as well as the differences of relative vorticity between asymmetric and symmetric vortices (Fig. 2c). Near the storm center, the streamfunction structure of the asymmetric vortex seems symmetric but tighter than that of the symmetric vortex. Away from the

TABLE 2. Experiment names and assimilation data types; N: *GOES-13/15* imager data are not assimilated; Y: *GOES-13/15* imager data are assimilated.

Experiment	Data type		Bogus vortex
	GOES-13/15	Other data	
CONTROL-S	N	AMSU-A,	Symmetric
GOES-S	Y	HIRS, AIRS,	Symmetric
CONTROL-AS	N	GPS RO, and	Asymmetric
GOES-AS	Y	conventional data	Asymmetric

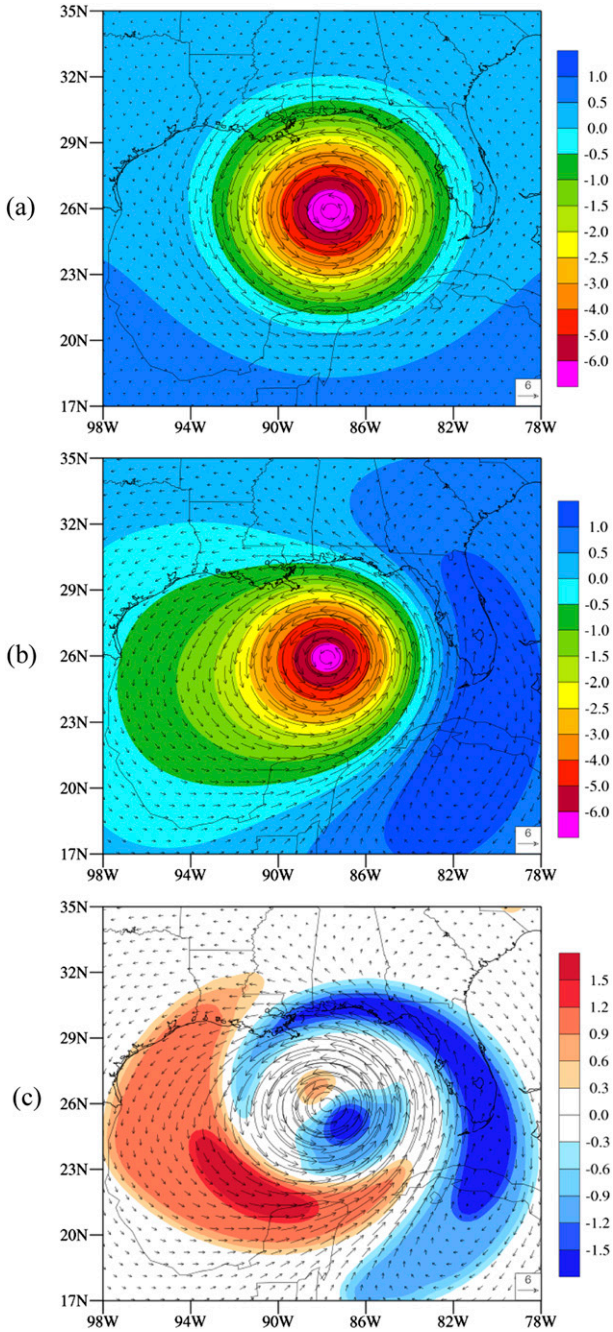

FIG. 2. Streamfunction (shaded; $10^6\,m^2\,s^{-1}$) and wind vectors (arrow; $m\,s^{-1}$) at 950 hPa of the (a) symmetric and (b) asymmetric initial bogus vortices for initializing Debby at 1800 UTC 23 Jun 2012. (c) Differences of relative vorticity between asymmetric and symmetric vortices (e.g., asymmetric minus symmetric).

storm center, the streamfunction exhibits an asymmetric structure, with positive streamfunction values extending toward the southwest and negative streamfunction values appearing in the northeast of the storm center (Fig. 2b). An asymmetric component is more clearly seen in the difference of the relative vorticity field between asymmetric and symmetric vortices (Fig. 2c). Near the storm center, a pair of negative and positive relative vorticity centers is aligned along the southeast and northwest directions. Farther away from the center, there is another pair of negative and positive relative vorticity centers aligned along the northeast and southwest directions with abroad azimuthal coverage. As mentioned before, such an asymmetric component of wind arises from the planetary vorticity advection by the symmetric flow of the symmetric vortex and is obtained by integrating a barotropic vorticity equation.

Figure 3a shows the vertical distribution of the tangential wind of the symmetric bogus vortex generated by the HWRF vortex initialization for Tropical Storm Debby at 1800 UTC 23 June 2012. The HWRF vortex is characterized by a symmetric cyclonic flow in the low and middle troposphere and an anticyclonic flow in the upper troposphere. The low-level horizontal distributions and cross sections of tangential and radial wind components of the asymmetric bogus vortex, which are used for initializing Debby at 1800 UTC 23 June 2012 in experiments CONTROL-AS and GOES-AS, are presented in Figs. 3b–e. A maximum area of tangential wind is located to the northeast of the vortex center (Fig. 3b). The cross section for the tangential wind component along the line passing through the vortex center and the maximum tangential wind location (Fig. 3d) shows a similar structure to the symmetric vortex (Fig. 3a) except for different magnitudes. The tangential wind in the east side of the vortex center (Fig. 3d) is stronger than that of the symmetric vortex (Fig. 3a), and the tangential wind in the west side of the vortex center (Fig. 3d) is weaker than that of the symmetric vortex (Fig. 3a). In contrast to the HWRF symmetric vortex for which the radial wind component is set to zero, the asymmetric vortex has a weak radial wind component, characterized by a large area of low-level inflow to the south of the vortex center and a small area of low-level outflow to the northwest of the vortex center (see Figs. 2b and 3e). The magnitude of the radial wind component decreases with altitude and the sign of the radial wind component does not change throughout the troposphere until above 160 hPa (Fig. 3e).

Both the symmetric (Figs. 2a and 3a) and asymmetric (Figs. 2b and 3b–e) vortices will be used for initializing the HWRF data assimilation cycling procedure, and their combined impacts on the track and intensity prediction of Tropical Storm Debby (2012) will be shown in section 5c.

b. *GOES data assimilation results*

GOES-13 and *-15* data are resampled, thinned, and converted to a meteorological data format called the

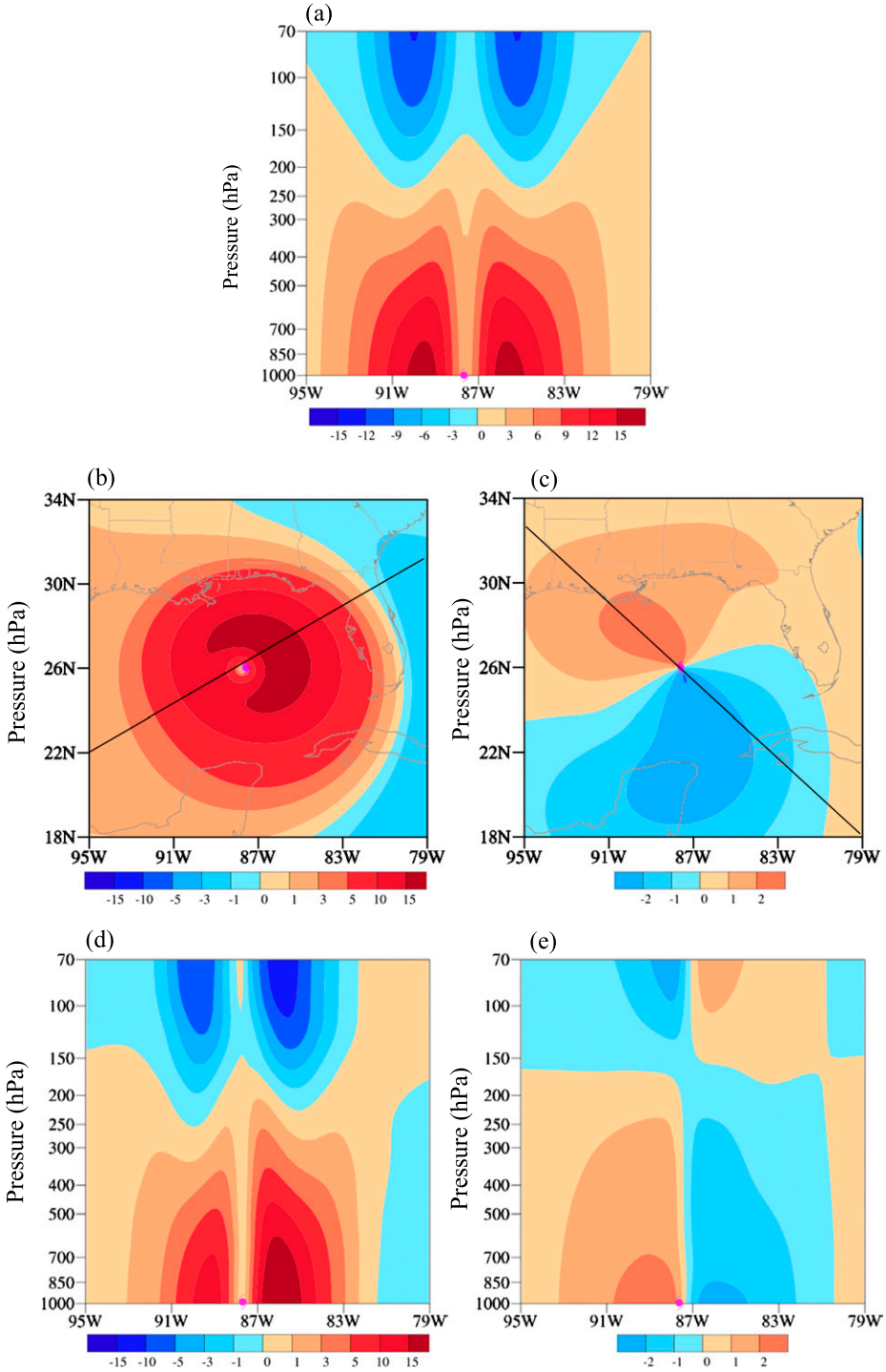

FIG. 3. (a) Cross section of tangential wind of the symmetric HWRF bogus vortex. (b),(c) Horizontal distributions at 950 hPa and (d),(e) cross sections of (left) tangential and (right) radial wind components of the asymmetric bogus vortex for initializing Debby at 1800 UTC 23 Jun 2012. The cross section in (d) for the tangential wind component is along the dotted black line in (b). The cross section in (e) for the radial wind component is along the dotted black line in (c). The observed storm center is indicated by a purple hurricane symbol.

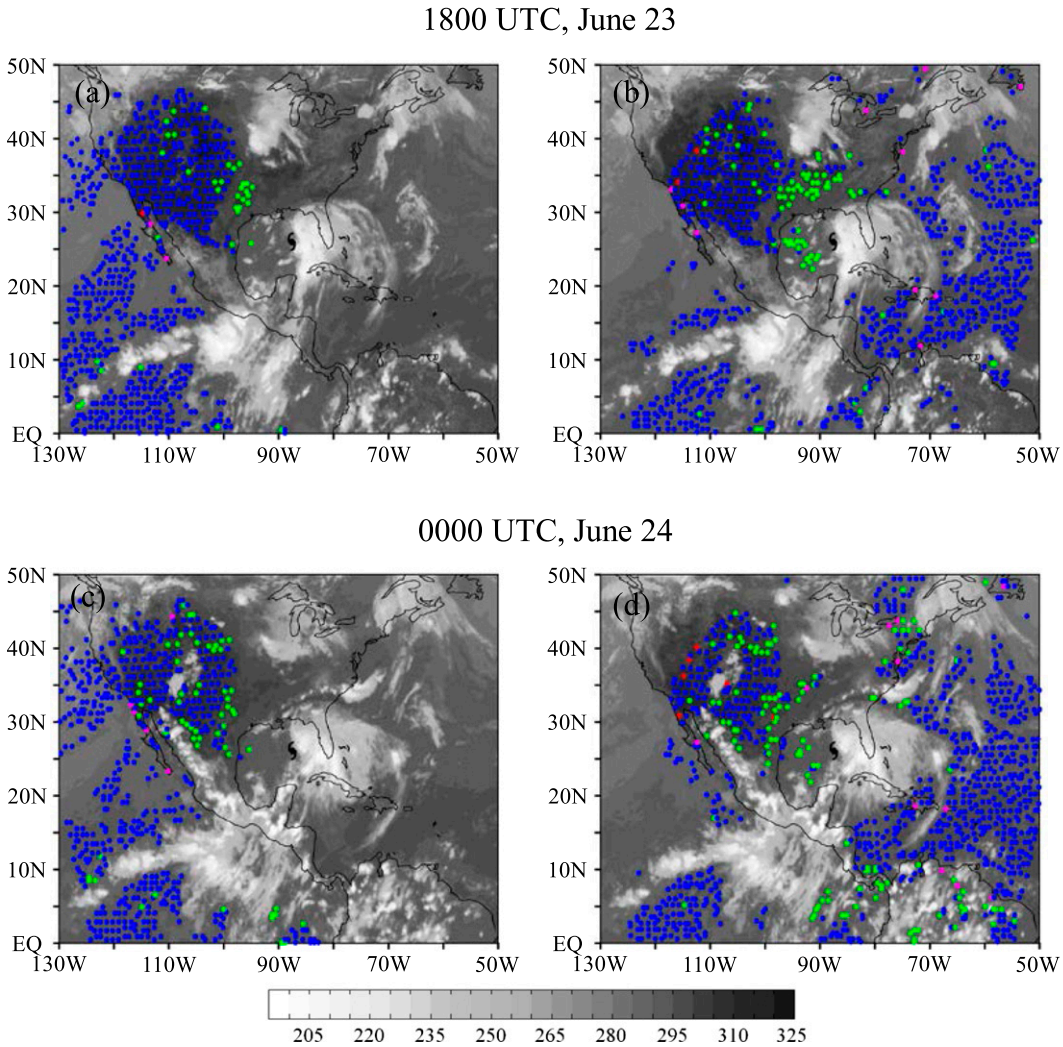

FIG. 4. Spatial distributions of channel 3 data points from (left) *GOES-15* and (right) *GOES-13* that pass (blue) and do not pass (magenta, red, green) QC in experiment GOES+AS at (a),(b) 1800 UTC 23 Jun and (c),(d) 0000 UTC 24 Jun 2012. Data removed by QC are based on surface type (magenta), large observation standard deviation (red), and large differences between observations and model simulations (green). GOES channel 4 brightness temperature observations are plotted in black/white shading.

Binary Universal Form for Representation of Meteorological Data (BUFR) and then fed into the GSI analysis system. The GOES BUFR data contain brightness temperature data, clear-sky fraction, and the standard deviation of the raw data within a thinned 40-km box for both *GOES-13* and *-15*. An advantage to using coarse-resolution radiances is that it reduces observation error correlation. The cloud mask algorithm developed by Heidinger (2011) was incorporated into the operational system. Data with a clear-sky fraction being less than 70% or a zenith angle greater than 60° are rejected. Additional quality control (QC) steps include rejecting data of the following types: (i) brightness temperatures are negative; (ii) channels 2, 4, and 6 over land; (iii) all channels over ice and snow surface; (iv) standard deviations of brightness temperature are greater than a prescribed value; and (v) differences of brightness temperature between observations and model simulations are more than 3 times the observation error. A detailed description of the GOES QC procedure was provided in the appendix of Zou et al. (2011).

It is pointed out that cloudy radiances were already removed in the GOES BUFR data. Figure 4 shows a series of spatial distributions of water vapor channel 3 data that are inputted into the HWRF/GSI system for both *GOES-13* and *-15* in experiment GOES+AS on 23 June 2012. Figure 5 is similar to Fig. 4 except for the

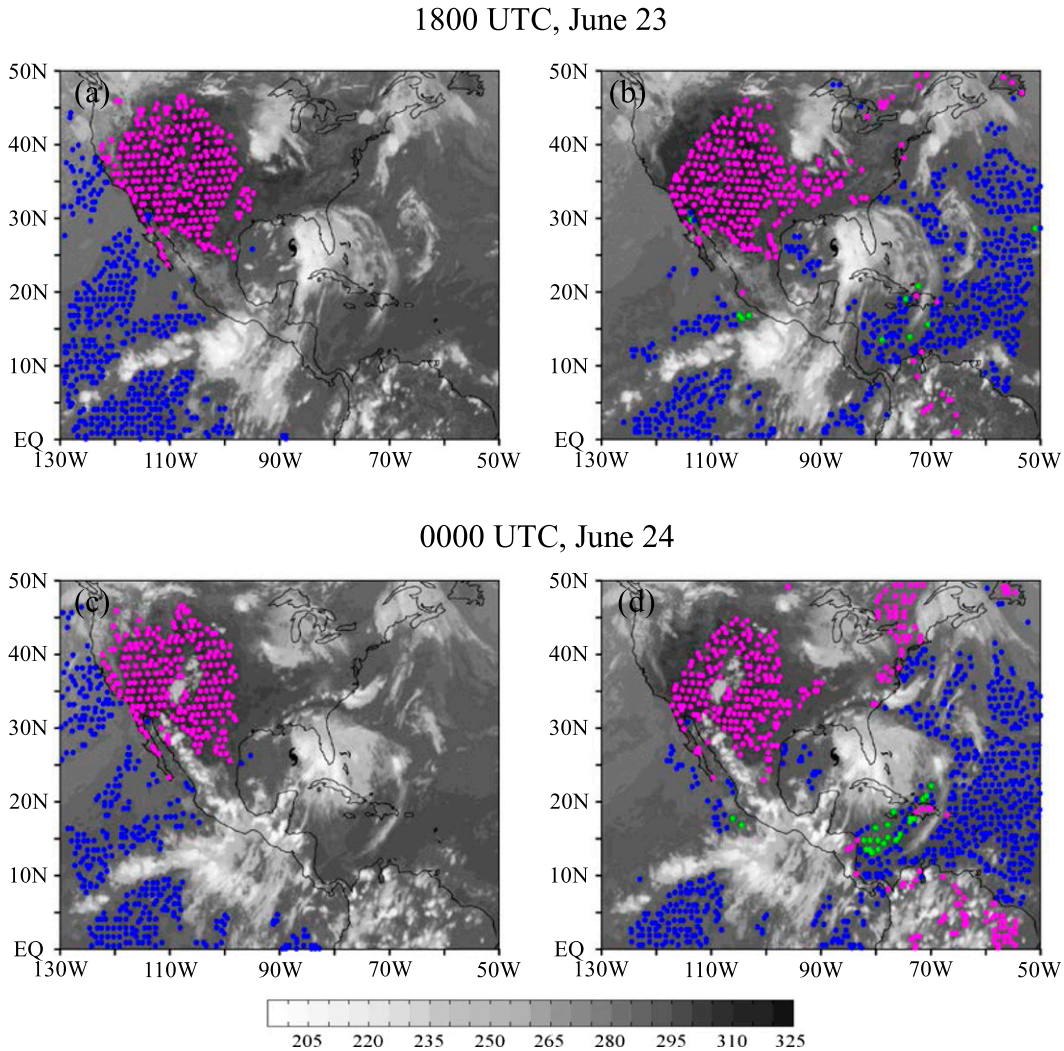

FIG. 5. As in Fig. 4, but for *GOES-13* channel 6.

CO_2 window channel 6. The brightness temperature observations of GOES channel 4 are plotted to indicate approximately the cloud distributions within and around Tropical Storm Debby. It is seen that the cloud detection that was applied to GOES data before they were inputted into the HWRF/GSI system did a reasonably good job in removing data points located in cloudy areas. Additional QC steps are applied to GOES BUFR data in the GSI system. The data points that pass QC and are assimilated into HWRF are indicated in blue, and data that do not pass QC are indicated in Figs. 4 and 5. Specifically, data that are removed by the QC procedure in the GSI system based on surface type, large observation standard deviations, and large differences between observations and model simulations are indicated in magenta, red, and green, respectively. As expected, GOES data within clouds are not assimilated. In the HWRF parent domain, most of the data from *GOES-15* overlap with those of *GOES-13* except for the midlatitude oceanic region near the West Coast. *GOES-13* provides unique data east of 90°W. A large amount of data is retained after the GSI QC for water vapor channel 3. A good coverage of the GOES water vapor channel in the clear-sky environment and clear streaks within clouds is found at both analysis times shown in Fig. 4. Similar results are found at other analysis times (figures omitted). For CO_2 window channel 6, all data over land are removed (Fig. 5). Over ocean, good coverage of GOES window channel data is also found in the clear-sky environment and clear streaks within clouds (Fig. 5).

The mean values and standard deviations of the differences between GOES observations (O) and model simulations before (e.g., $O - B$) and after (e.g., $O - A$)

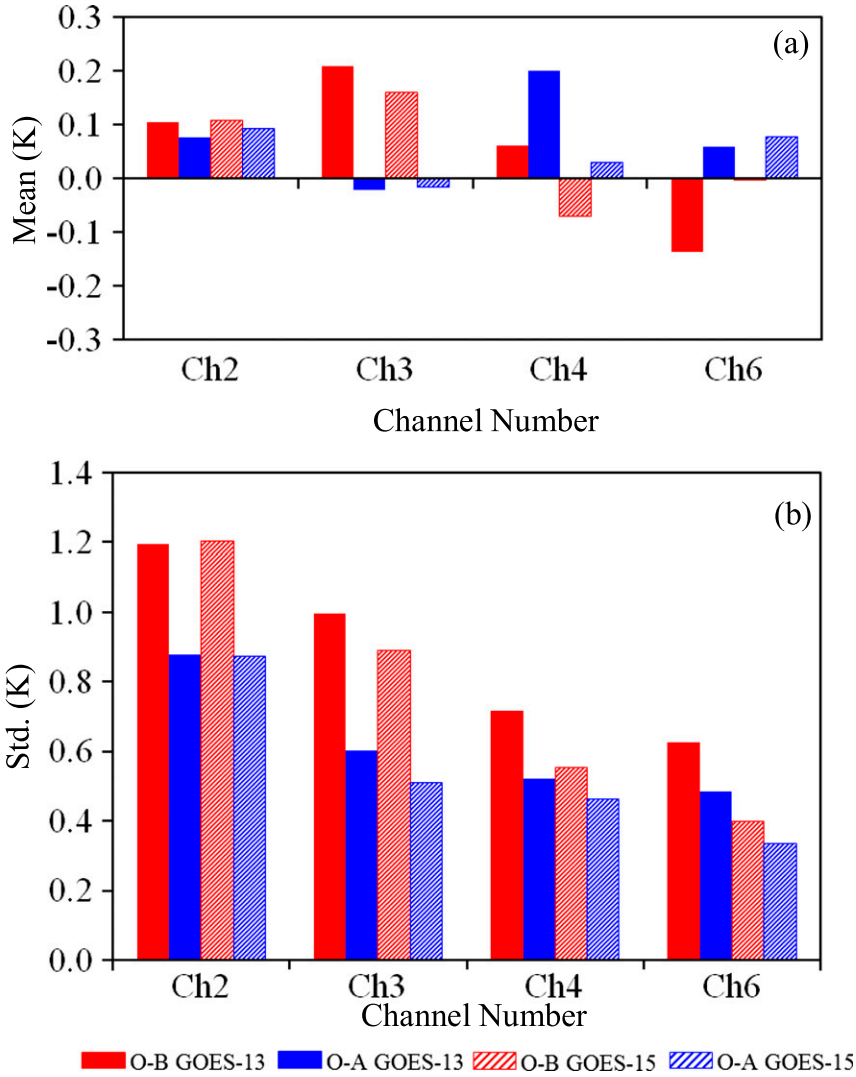

FIG. 6. (a) Mean and (b) standard deviation of $O - B$ (red) and $O - A$ (blue) for *GOES-13* (solid bar) and *GOES-15* (dashed bar) in experiment GOES+AS from 1800 UTC 23 Jun to 1800 UTC 24 Jun 2012.

GOES data assimilation for both *GOES-13* and *GOES-15* in experiment GOES+AS during the time period from 1800 UTC 23 June to 1800 UTC 24 June 2012 are provided in Fig. 6, where brightness temperature simulations from background fields are denoted B and those simulated from analysis fields are denoted A. Large positive biases are found in the background fields for water vapor channel 3 of both *GOES-13* and *-15* (Fig. 6a). The largest negative bias is found for channel 6 from *GOES-13*, which is significantly reduced after GOES data assimilation (Fig. 6a). Standard deviations between observations and model simulations are generally reduced by data assimilation (Fig. 6b).

To confirm that the large positive bias in channel 3 and the large negative bias in channel 6 are present at all analysis times, the spatial distributions of $O - B$ and $O - A$ of *GOES-13* channels 3 and 6 are shown in Figs. 7 and 8 at 6-h intervals for the time period from 0000 UTC to 1800 UTC 24 June 2012 in experiment GOES+AS. It is seen that a few degrees of positive $O - B$ values in channel 3 are not only at all analysis times but also prevail throughout the entire model domain (Fig. 7, left panels). Similarly, a few degrees of negative $O - B$ values in channel 6 are seen at all analysis times and within the entire model domain (Fig. 8, left panels). After GOES data assimilation, the differences between the observations and model simulations are significantly reduced to within ± 1 K (Figs. 7 and 8, right panels).

A more precise way of examining the convergence of GOES data assimilation is to examine the values of

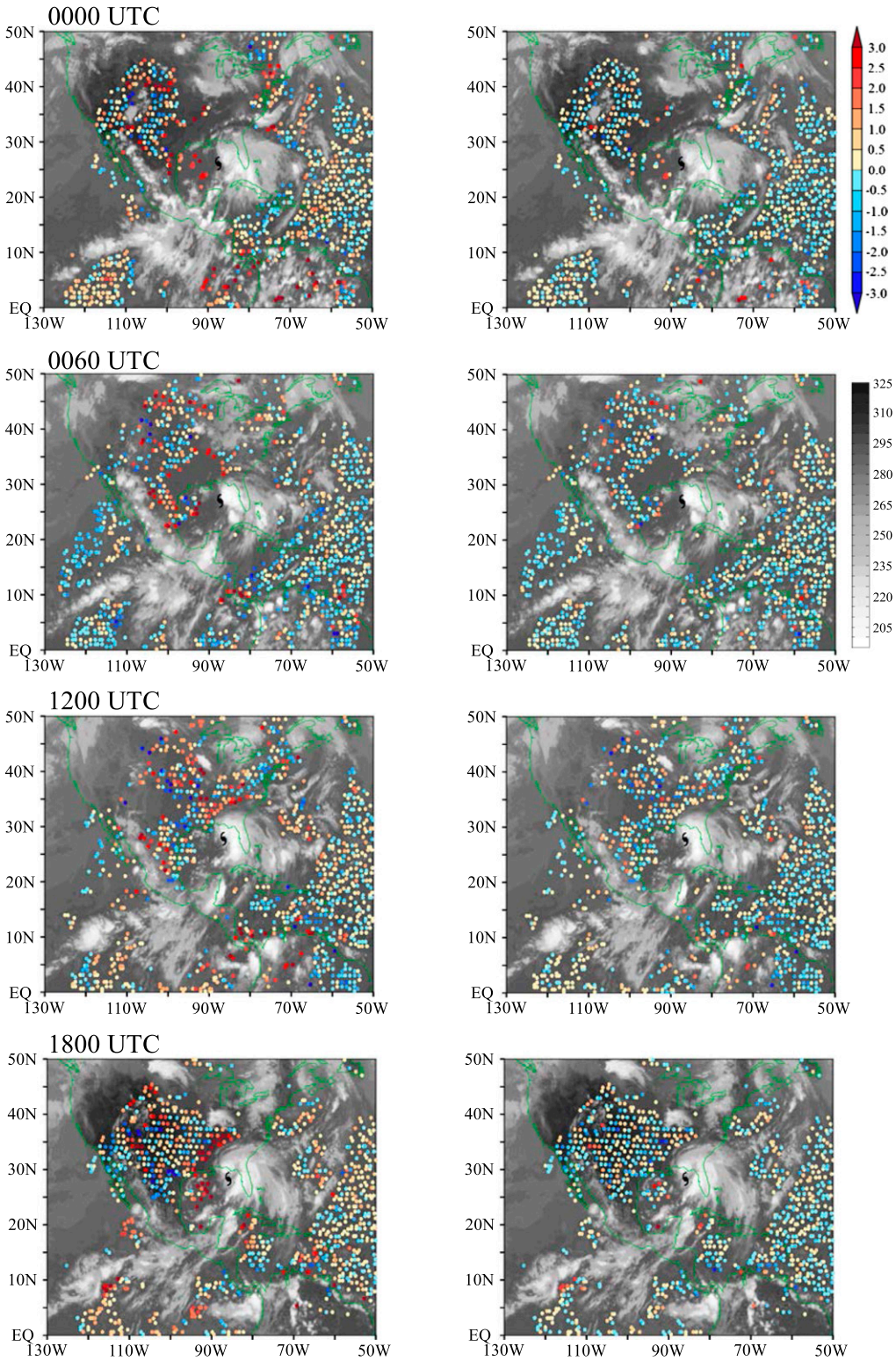

FIG. 7. Spatial distributions of (left) $O - B$ and (right) $O - A$ of *GOES-13* channel 3 on 23 Jun 2012 at 6-h intervals in experiment GOES+AS. The magnitudes of $O - B$ and $O - A$ are color-coded (K). GOES channel 4 brightness temperature observations are plotted in black/white shading.

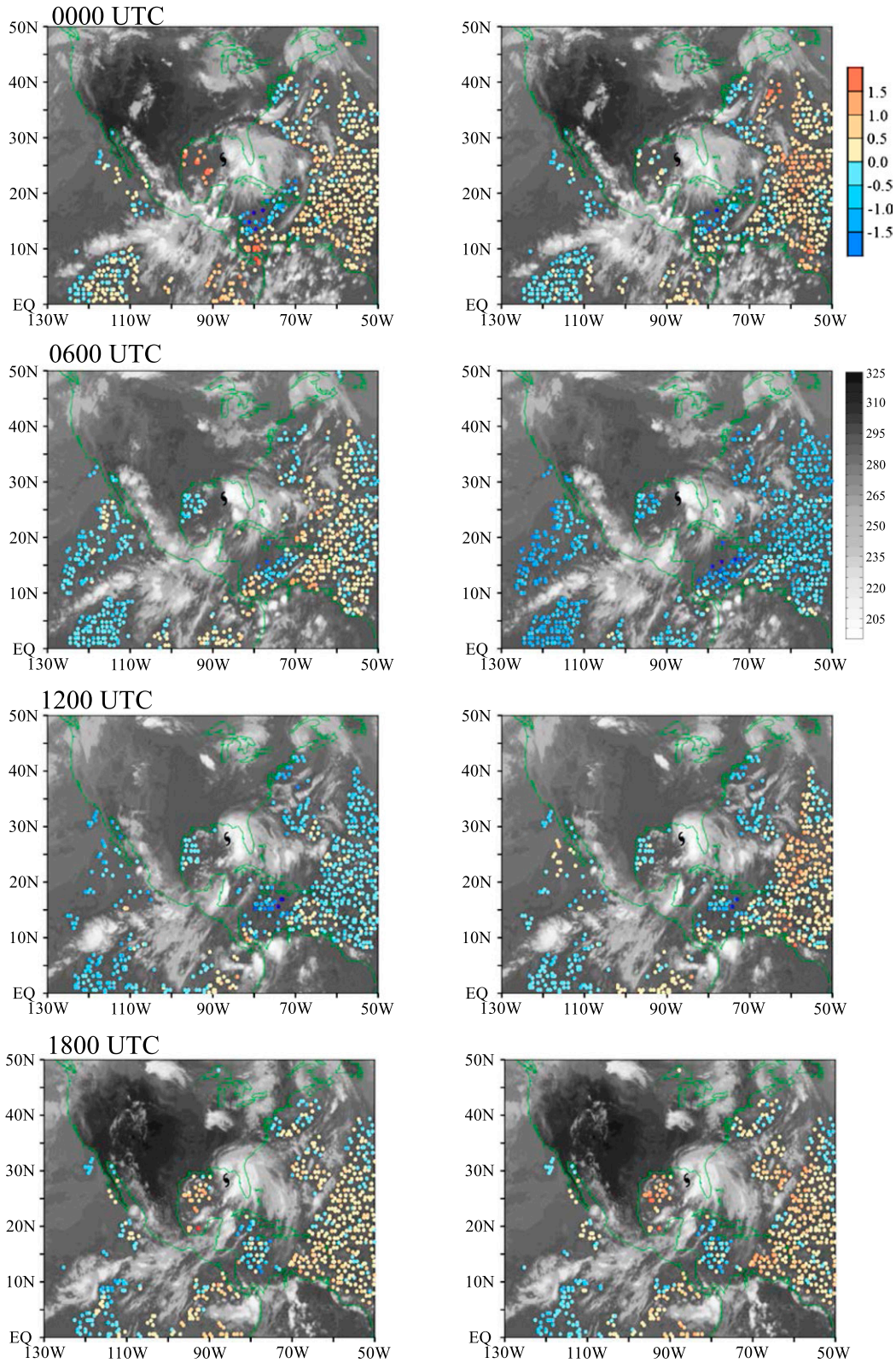

FIG. 8. As in Fig. 7, but for *GOES-13* channel 6.

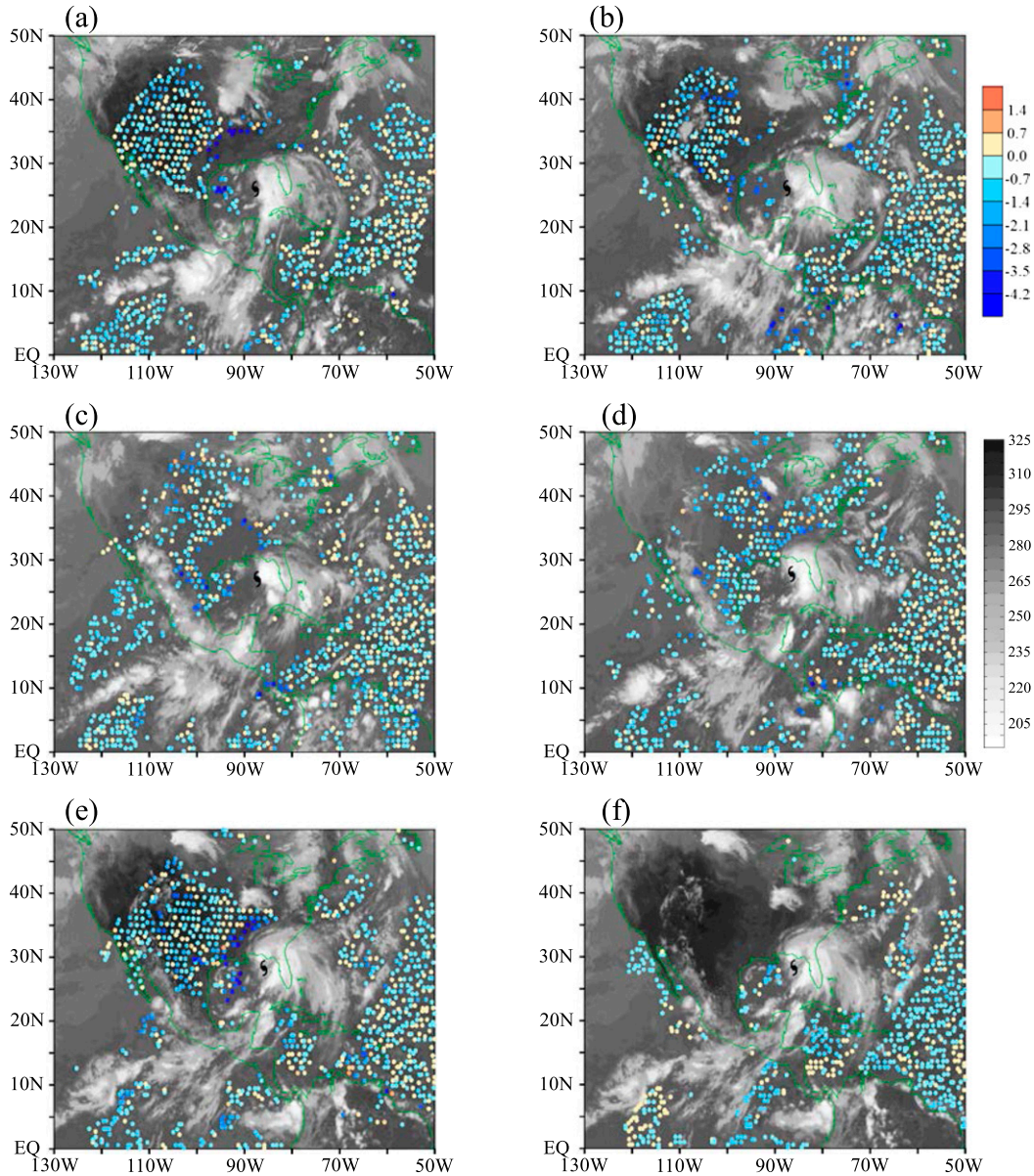

FIG. 9. Spatial distribution of *GOES-13* channel 6 for experiment GOES+AS from 1800 UTC 23 Jun to 0000 UTC 25 Jun 2012 at 6-h intervals. Data colored with $|O-A|-|O-B|$.

$|O-A|-|O-B|$ at all GOES data points assimilated in the HWRF system. Figure 9 shows the spatial distribution of *GOES-13* channel 3 for experiment GOES+AS from 1800 UTC 23 June to 0000 UTC 25 June 2012 at 6-h intervals. A negative value of $|O-A|-|O-B|$ indicated a closer fit of model simulation to GOES observation after GOES radiance assimilation. Results in Fig. 9 confirm a systematic convergence of GOES data assimilation for channel 3 at all analysis times and all data points, especially for data points near the storm center.

Having shown the differences between model simulations and GOES observations in observation space (Figs. 4–9), differences of geopotential analysis at 300 hPa with and without (CONTROL+AS) GOES data assimilation—that is, GOES+AS minus CONTROL+AS—at 1800 UTC 23 June 2012 are presented in Fig. 10. At 300 hPa, two positive differences of around 6 m are seen near the storm center (Fig. 10a). Such a difference in geopotential fields resulting from GOES data assimilation extends from about 500 to around 50 hPa. The maximum difference is located around 300 hPa (Fig. 10b). The differences of temperature with and without GOES data assimilation along an across section cutting through the storm center from west to east is also provided in

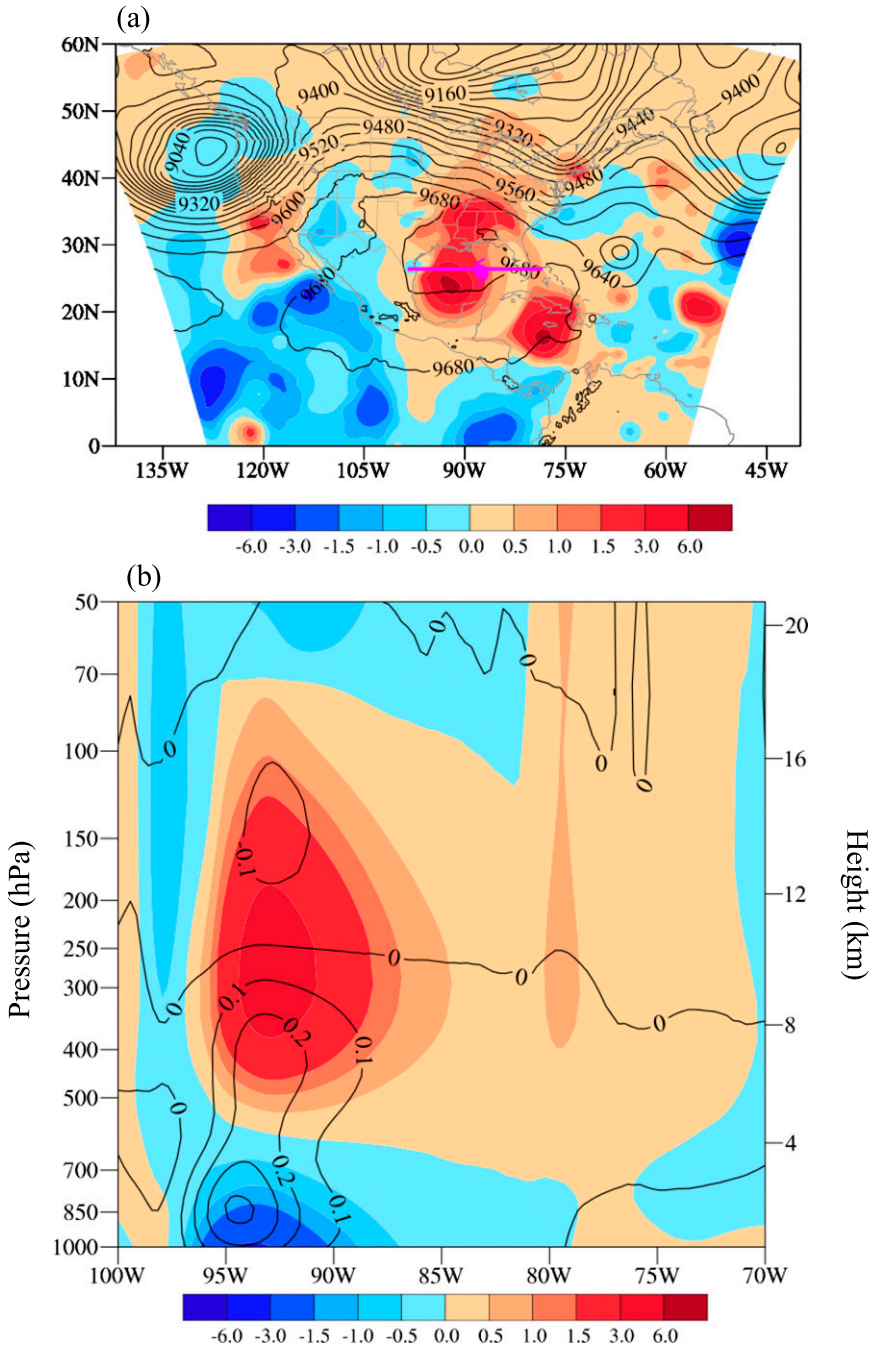

FIG. 10. (a) Geopotential at 300 hPa of experiment GOES+AS (black contour; m) and the differences of geopotential at 300 hPa with (GOES+AS) and without (CONTROL+AS) GOES data assimilation (color shading). (b) Cross section of the differences of temperature (black contour; K) and geopotential at 300 hPa with (GOES+AS) and without (CONTROL+AS) GOES data assimilation (color shading) at 1800 UTC 23 Jun 2012 along the pink line indicated in (a). The observed storm center is indicated by a hurricane symbol in purple.

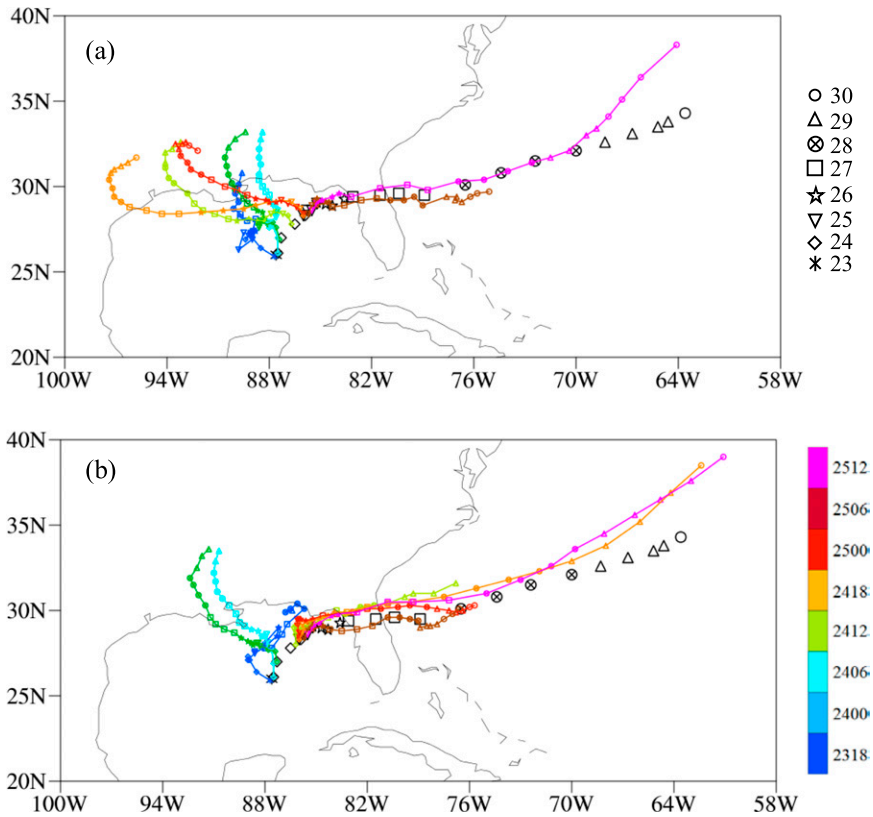

FIG. 11. Observed (black) and forecast (color) tracks of Tropical Storm Debby from 1800 UTC 23 Jun 2012 to 1200 UTC 25 Jun 2012 (a) without and (b) with GOES imager data assimilation. An asymmetric vortex initialization is incorporated. Color bars show the initial dates of different forecasts, and symbols show the different dates of observations.

Fig. 10b. A warm center of about 0.3 K is generated between 300 and 600 hPa by GOES data assimilation (Fig. 10b). The differences in analyses resulting from GOES data assimilation will affect the track and intensity forecasts of Debby, which are shown below.

c. *Impacts on track and intensity forecasts*

The observed and model-forecasted tracks of Tropical Storm Debby from CONTROL-AS, which has an asymmetric initial vortex initialization but without GOES imager data assimilation, are presented in Fig. 11a. Figure 11b is the same as Fig. 11a except for GOES+AS, in which GOES imager data assimilation is carried out with an asymmetric initial vortex. While the observed Debby moved eastward, model forecasts initialized at and before 0000 UTC 25 June 2012 produced a set of northwestward tracks in CONTROL+AS (Fig. 11a). Adding GOES imager radiance observations to the assimilation of other types of data produced an eastward track prediction more than a half day earlier than the control experiment (CONTROL+AS, Fig. 11b). The mean and root-mean-square track errors of model forecasts initialized from 1800 UTC 23 June to 1200 UTC 25 June 2012 for Tropical Storm Debby by the experiments without and with GOES data assimilation and with and without asymmetric component in the initial—that is, CONTROL+S, GOES+S, CONTROL+AS, GOES+AS—are shown in Fig. 12. GOES imager data assimilation reduces the track error for both the symmetric and asymmetric vortex initialization schemes. The GOES+AS experiment outperforms the other three experiments in terms of both the mean errors and standard deviations of the track predictions.

The main reason for the difference in track predictions among four experiments is probably associated with the model forecasts of the subtropical high. Figure 13 shows the HWRF analysis of geopotential and wind vector at 500 hPa valid at 1800 UTC 24 June 2012 from the above four numerical experiments. The area with the geopotential being greater than 5880 m in GOES-AS is clearly broader than those from the other three forecasts. This would alter the environmental steering of modeled Hurricane Debby. A stronger

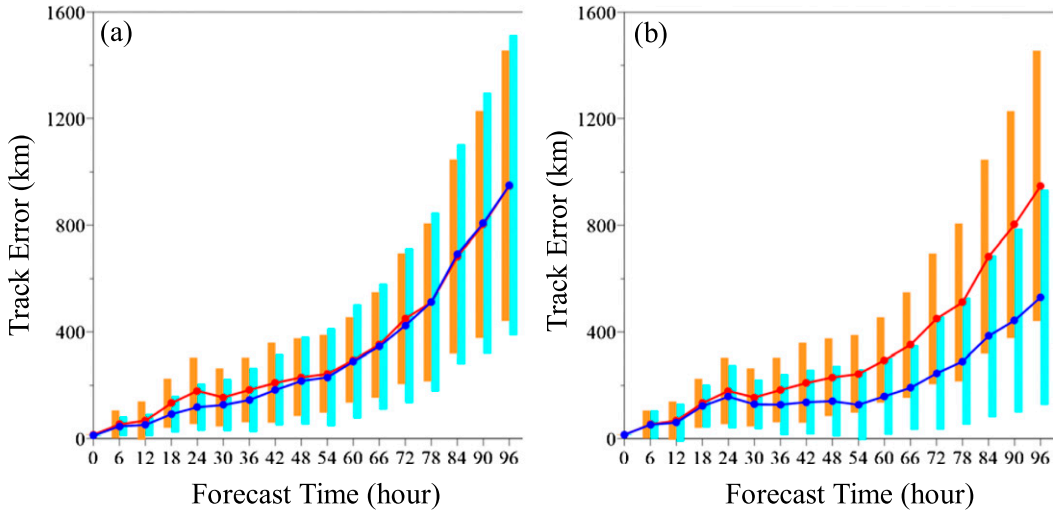

FIG. 12. Mean errors (curves with dots) and root-mean-square errors (vertical bars) of model forecasts initialized from 1800 UTC 23 Jun to 1200 UTC 25 Jun 2012 for Tropical Storm Debby by the experiments without (red and orange) and with (blue and cyan) GOES data assimilation with (a) symmetric and (b) asymmetric vortex initialization.

geopotential high at the east side of the tropical storm corresponds to a stronger anticyclonic circulation. The southwestward flows on the west side of the subtropical high would steer the storm eastward.

The combined impacts of *GOES-13/15* imager radiance assimilation and asymmetric vortex initialization on intensity forecasts are shown in Figs. 14 and 15. The model-predicted central sea level pressure (SLP) (Fig. 14) and the maximum surface wind (Fig. 15) from the GOES+AS experiment approximate the observed values of storm Debby most closely throughout the 4-day forecast period. The asymmetric vortex initialization allowed the GOES imager radiance assimilation to have more significant positive impacts on the

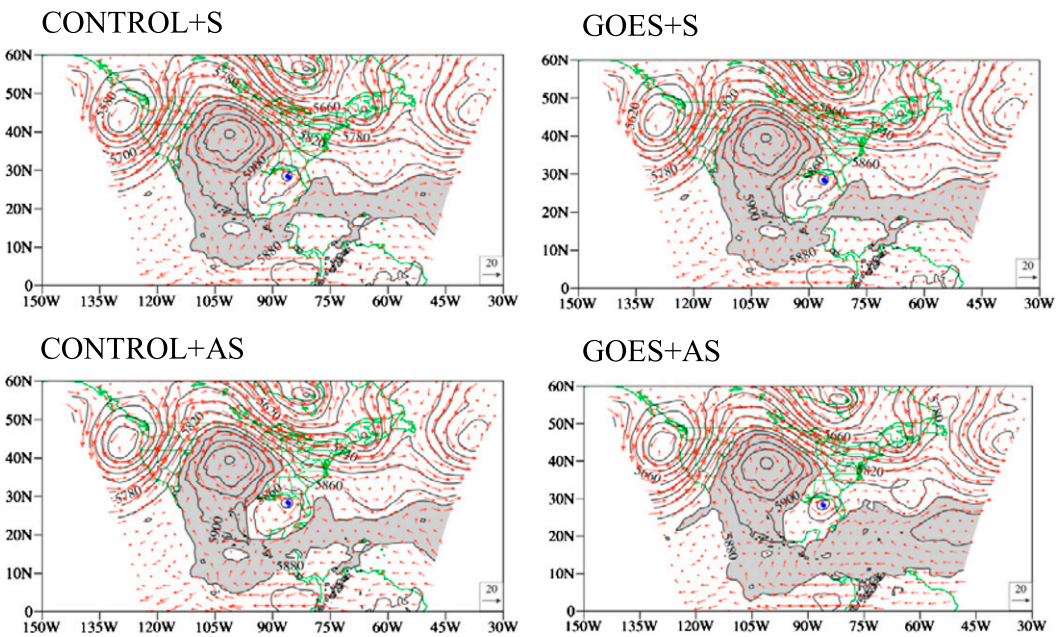

FIG. 13. Geopotential (black contour; m) and wind vector (red vector; m s^{-1}) at 500 hPa valid at 1800 UTC 23 Jun 2012 (left) without and (right) with GOES imager data assimilated for the experiments with (top) symmetric and (bottom) asymmetric vortex initialization schemes. Areas with the geopotential greater than 5880 m are shaded.

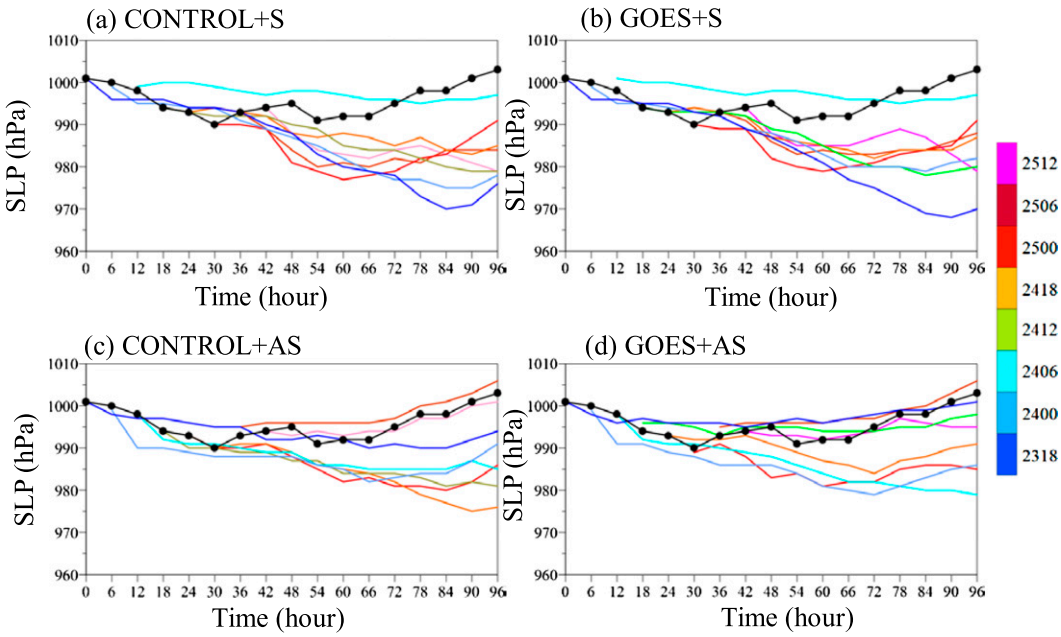

FIG. 14. Observed (black dotted line) and predicted central SLP of Debby for experiments (left) without and (right) with GOES data assimilation with (a),(b) symmetric and (c),(d) asymmetric vortex initialization. Starting point on the *x* axis corresponds to 1800 UTC 23 Jun 2012.

storm's intensity forecasts than the symmetric vortex initialization.

6. Summary and conclusions

The present study provides a preliminary assessment of the added values of GOES imager radiance assimilation for improved track and intensity forecasts using the HWRF system. Although having only one water vapor sounding channel and three window channels, *GOES-13* and *-15* data are available at all analysis times and have high spatial and temporal resolutions. The GOES imager radiance measurements are directly assimilated by the NCEP GSI embedded in the HWRF

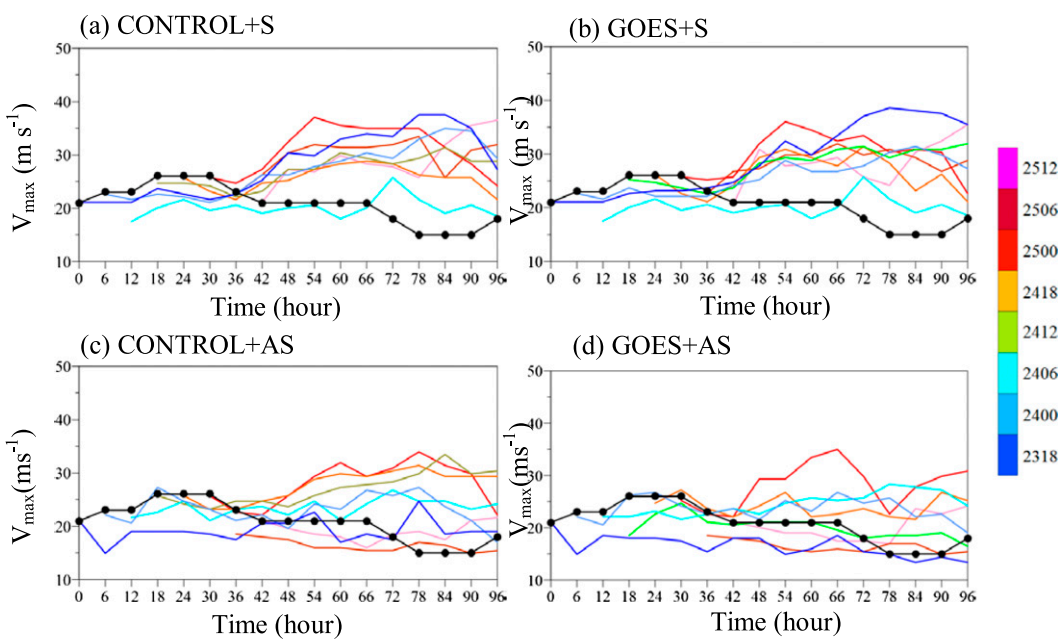

FIG. 15. As in Fig. 14, but for the maximum surface wind speed.

system. The added values of GOES radiances to conventional and three other types of satellite instruments (i.e., AMSU-A, AIRS, and HIRS) for improved tropical storm forecasts over the Gulf of Mexico are compared with symmetric and asymmetric vortex initialization schemes. It is found that GOES radiance data assimilation in the HWRF system contributes positively to both the track and intensity forecasts. The improvements brought by the GOES data assimilation are more significant when an asymmetric vortex initialization scheme is incorporated into the HWRF system.

This study only investigated impacts of a direct assimilation of GOES radiance observations for a real tropical storm case. Impacts of GOES radiance assimilation experiments on hurricane track and intensity forecasts could be case dependent. More case studies are required for generalizing the conclusions drawn from this study on the impacts of GOES radiance assimilation for improved tropical cyclone forecasts. Further improvements can be made to GOES data assimilation. Currently, GOES data over land were not assimilated except for channel 3. A further study is planned to diagnose and improve the assimilation of GOES surface-sensitive channels, especially channels 2 and 4. Channels 2 (3.9 μm) and 4 (10.7 μm) are considerably more difficult to assimilate than the other two GOES channels (i.e., channels 3 and 6) due to the fact that channel 2 is significantly affected by solar contamination and both channels 2 and 4 have larger uncertainty with their surface emissivity. Finally, a separate but related study is being carried out to assess if adding GOES satellite data assimilation can improve the hurricane forecast skill by as much as an early morning polar-orbit satellite, such as *NOAA-15*. Such an assessment is important, since *NOAA-15* has already been flown for more than 16 years.

Acknowledgments. This work was jointly supported by the Chinese Ministry of Science and Technology Project 2015CB452805, NOAA GOES-R Risk Reduction Program Project NA11OAR4320199, and the Natural Science Foundation of China Project 41475103.

REFERENCES

Amerault, C., and J. Doyle, 2008: Assimilation of small scale observations with a nested adjoint model. *Atmospheric and Environmental Remote Sensing Data Processing and Utilization IV: Readiness for GEOSS II,* M. D. Goldberg et al., Eds., International Society for Optical Engineering (SPIE Proceedings, Vol. 7085), 70850R, doi:10.1117/12.795348.

——, X. Zou, and J. Doyle, 2009: Assimilation of rain-affected radiances with an adjoint model. *J. Appl. Remote Sens.,* **3,** 033531, doi:10.1117/1.3153332.

Andersson, E., J. Pailleux, J.-N. Thépaut, J. R. Eyre, A. P. McNally, G. A. Kelly, and P. Courtier, 1994: Use of cloud-cleared radiances in three/four-dimensional variational data assimilation. *Quart. J. Roy. Meteor. Soc.,* **120,** 627–653, doi:10.1002/qj.49712051707.

Bao, S., R. Yablonsky, D. Stark, and L. Bernardet, 2012: Community HWRF users guide V3.4a. Developmental Testbed Center Tech. Memo. OAR GSD-42, 124 pp.

Bender, M. A., R. J. Ross, R. E. Tuleya, and Y. Kurihara, 1993: Improvements in tropical cyclone track and intensity forecasts using the GFDL initialization system. *Mon. Wea. Rev.,* **121,** 2046–2061, doi:10.1175/1520-0493(1993)121<2046:IITCTA>2.0.CO;2.

Derber, J. C., and W.-S. Wu, 1998: The use of TOVS cloud-cleared radiances in the NCEP SSI analysis system. *Mon. Wea. Rev.,* **126,** 2287–2299, doi:10.1175/1520-0493(1998)126<2287:TUOTCC>2.0.CO;2.

Eyre, J. R., G. Kelly, A. P. McNally, E. Andersson, and A. Persson, 1993: Assimilation of TOVS radiance information through one-dimensional variational analysis. *Quart. J. Roy. Meteor. Soc.,* **119,** 1427–1463, doi:10.1002/qj.49711951411.

Goerss, J. S., C. S. Velden, and J. D. Hawkins, 1998: The impact of multispectral *GOES-8* wind information on Atlantic tropical cyclone forecasts in 1995. Part II: NOGAPS forecasts. *Mon. Wea. Rev.,* **126,** 1219–1227, doi:10.1175/1520-0493(1998)126<1219:TIOMGW>2.0.CO;2.

Gopalakrishnan, S., S. Goldenberg, T. Quirino, F. Marks, X. Zhang, K.-S. Yeh, R. Atlas, and V. Tallapragada, 2012: Towards improving high-resolution numerical hurricane forecasting: Influence of model horizontal grid resolution, initialization, and physics. *Wea. Forecasting,* **27,** 647–666, doi:10.1175/WAF-D-11-00055.1.

——, and Coauthors, 2012: Hurricane Weather Research and Forecasting (HWRF) Model: 2012 science documentation. HWRF v3.4a, Developmental Testbed Center Tech. Rep., 96 pp.

Han, Y., F. Weng, Q. Liu, and P. van Delst, 2007: A fast radiative transfer model for SSMIS upper atmosphere sounding channels. *J. Geophys. Res.,* **112,** D11121, doi:10.1029/2006JD008208.

Heidinger, A., 2011: NOAA NESDIS Center for Satellite Applications and Research algorithm theoretical basis document: ABI cloud mask. Version 2.0, 93 pp.

Janjić, Z. I., 2003: A nonhydrostatic model based on a new approach. *Meteor. Atmos. Phys.,* **82,** 271–285, doi:10.1007/s00703-001-0587-6.

——, J. P. Gerrity, and S. Nickovic, 2001: An alternative approach to nonhydrostatic modeling. *Mon. Wea. Rev.,* **129,** 1164–1178, doi:10.1175/1520-0493(2001)129<1164:AAATNM>2.0.CO;2.

Köpken, C., G. Kelly, and J.-N. Thépaut, 2004: Assimilation of Meteosat radiance data within the 4D-Var system at ECMWF: Assimilation experiments and forecast impact. *Quart. J. Roy. Meteor. Soc.,* **130,** 2277–2292, doi:10.1256/qj.02.230.

Kurihara, Y., M. A. Bender, and R. J. Ross, 1993: An initialization scheme of hurricane models byvortex specification. *Mon. Wea. Rev.,* **121,** 2030–2045, doi:10.1175/1520-0493(1993)121<2030:AISOHM>2.0.CO;2.

——, ——, R. E. Tuleya, and R. J. Ross, 1995: Improvements in the GFDL Hurricane Prediction System. *Mon. Wea. Rev.,* **123,** 2791–2801, doi:10.1175/1520-0493(1995)123<2791:IITGHP>2.0.CO;2.

McNally, A. P., and Coauthors, 2006: The assimilation of AIRS radiance data at ECMWF. *Quart. J. Roy. Meteor. Soc.,* **132,** 935–957, doi:10.1256/qj.04.171.

Migliorini, S., 2012: On the equivalence between radiance and retrieval assimilation. *Mon. Wea. Rev.,* **140,** 258–265, doi:10.1175/MWR-D-10-05047.1.

Nieman, S. J., J. Schmetz, and W. P. Menzel, 1993: A comparison of several techniques to assign heights to cloud tracers. *J. Appl. Meteor.,* **32,** 1559–1568, doi:10.1175/1520-0450(1993)032<1559:ACOSTT>2.0.CO;2.

Pu, Z., X. Li, and J. Sun, 2009: Impact of airborne Doppler radar data assimilation on the numerical simulation of intensity changes of Hurricane Dennis near a landfall. *J. Atmos. Sci.,* **66,** 3351–3365, doi:10.1175/2009JAS3121.1.

Purser, R. J., W.-S. Wu, D. F. Parrish, and N. M. Roberts, 2003a: Numerical aspects of the application of recursive filters to variational statistical analysis. Part I: Spatially homogeneous and isotropic Gaussian covariances. *Mon. Wea. Rev.,* **131,** 1524–1535, doi:10.1175/1520-0493(2003)131<1524:NAOTAO>2.0.CO;2.

——, ——, ——, and ——, 2003b: Numerical aspects of the application of recursive filters to variational statistical analysis. Part II: Spatially inhomogeneous and anisotropic general covariances. *Mon. Wea. Rev.,* **131,** 1536–1548, doi:10.1175/2543.1.

Qin, Z., X. Zou, and F. Weng, 2013: Evaluating added benefits of assimilating GOES imager radiance data in GSI for coastal QPFs. *Mon. Wea. Rev.,* **141,** 75–92, doi:10.1175/MWR-D-12-00079.1.

Rao, P. A., C. S. Velden, and S. A. Braun, 2002: The vertical error characteristics of GOES-derived winds: Description and experiments with numerical weather prediction. *J. Appl. Meteor.,* **41,** 253–271, doi:10.1175/1520-0450(2002)041<0253:TVECOG>2.0.CO;2.

Soden, B. J., C. S. Velden, and R. E. Tuleya, 2001: The impact of satellite winds on experimental GFDL hurricane model forecasts. *Mon. Wea. Rev.,* **129,** 835–852, doi:10.1175/1520-0493(2001)129<0835:TIOSWO>2.0.CO;2.

Stengel, M., P. Undén, M. Lindskog, P. Dahlgren, N. Gustafsson, and R. Bennartz, 2009: Assimilation of SEVIRI infrared radiances with HIRLAM 4D-Var. *Quart. J. Roy. Meteor. Soc.,* **135,** 2100–2109, doi:10.1002/qj.501.

Su, X., J. Derber, J. Jung, Y. Tahara, D. Keyser, and R. Treadon, 2003: The usage of GOES imager clear-sky radiance in the NCEP Global Data Assimilation System. Preprints, *12th Conf. on Satellite Meteorological and Oceanography,* Long Beach, CA, Amer. Meteor. Soc., P3.20. [Available online at https://ams.confex.com/ams/annual2003/techprogram/paper_56361.htm.]

Szyndel, M. D. E., J.-N. Thépaut, and G. Kelly, 2005: Evaluation of potential benefit of SEVIRI water vapour radiance data from Meteosat-8 into global numerical weather prediction analyses. *Atmos. Sci. Lett.,* **6,** 105–111, doi:10.1002/asl.98.

Tomassini, M., G. Kelly, and R. Saunders, 1999: Use and impact of satellite atmospheric motion winds on ECMWF analyses and forecasts. *Mon. Wea. Rev.,* **127,** 971–986, doi:10.1175/1520-0493(1999)127<0971:UAIOSA>2.0.CO;2.

Velden, C. S., 1996: Winds derived from geostationary satellite moisture channel observations: Applications and impact on numerical weather prediction. *Meteor. Atmos. Phys.,* **60,** 37–46, doi:10.1007/BF01029784.

——, C. M. Hayden, S. J. Nieman, W. P. Menzel, S. Wazong, and J. S. Goerss, 1997: Upper-tropospheric winds derived from geostationary satellite water vapor observations. *Bull. Amer. Meteor. Soc.,* **78,** 173–195, doi:10.1175/1520-0477(1997)078<0173:UTWDFG>2.0.CO;2.

——, T. L. Olander, and S. Wazong, 1998: The impact of multispectral *GOES-8* wind information on Atlantic tropical cyclone track forecasts in 1995. Part I: Dataset methodology, description and case analysis. *Mon. Wea. Rev.,* **126,** 1202–1218, doi:10.1175/1520-0493(1998)126<1202:TIOMGW>2.0.CO;2.

Weng, F., 2007: Advances in radiative transfer modeling in support of satellite data assimilation. *J. Atmos. Sci.,* **64,** 3799–3807, doi:10.1175/2007JAS2112.1.

Wu, W.-S., R. J. Purser, and D. F. Parrish, 2002: Three-dimensional variational analysis with spatially inhomogeneous covariances. *Mon. Wea. Rev.,* **130,** 2905–2916, doi:10.1175/1520-0493(2002)130<2905:TDVAWS>2.0.CO;2.

Zhang, F., and Y. Weng, 2015: Predicting hurricane intensity and associated hazards: A five-year real-time forecast experiment with the assimilation of airborne Doppler radar observations. *Bull. Amer. Meteor. Soc.,* **96,** 25–33, doi:10.1175/BAMS-D-13-00231.1.

——, ——, J. F. Gamache, and F. D. Marks, 2011: Performance of convection-permitting hurricane initialization and prediction during 2008–2010 with ensemble data assimilation of inner-core airborne Doppler radar observations. *Geophys. Res. Lett.,* **38,** L15810, doi:10.1029/2011GL048469.

Zhu, T., D.-L. Zhang, and F. Weng, 2002: Impact of the Advanced Microwave Sounding Unit measurements on hurricane prediction. *Mon. Wea. Rev.,* **130,** 2416–2432, doi:10.1175/1520-0493(2002)130<2416:IOTAMS>2.0.CO;2.

Zou, X., and Q. Xiao, 2000: Studies on the initialization and simulation of a mature hurricane using a variational bogus data assimilation scheme. *J. Atmos. Sci.,* **57,** 836–860, doi:10.1175/1520-0469(2000)057<0836:SOTIAS>2.0.CO;2.

——, ——, A. E. Lipton, and G. D. Modica, 2001: A numerical study of the effect of GOES sounder cloud-cleared brightness temperatures on the prediction of hurricane Felix. *J. Appl. Meteor.,* **40,** 34–55, doi:10.1175/1520-0450(2001)040<0034:ANSOTE>2.0.CO;2.

——, Z. Qin, and F. Weng, 2011: Improved coastal precipitation forecasts with direct assimilation of *GOES-11/12* imager radiances. *Mon. Wea. Rev.,* **139,** 3711–3729, doi:10.1175/MWR-D-10-05040.1.

——, F. Weng, B. Zhang, L. Lin, Z. Qin, and V. Tallapragada, 2013: Impacts of assimilation of ATMS data in HWRF on track and intensity forecasts of 2012 four landfall hurricanes. *J. Geophys. Res. Atmos.,* **118,** 11 558–11 576, doi:10.1002/2013JD020405.